Article

Hydrogenation of N-Heteroarenes Using Rhodium Precatalysts: Reductive Elimination Leads to Formation of Multimetallic Clusters

Sangmin Kim, Florian Loose, Máté J. Bezdek, Xiaoping Wang, and Paul J. Chirik

J. Am. Chem. Soc., **Just Accepted Manuscript** • DOI: 10.1021/jacs.9b09540 • Publication Date (Web): 07 Oct 2019

Hydrogenation of *N*-Heteroarenes Using Rhodium Precatalysts: Reductive Elimination Leads to Formation of Multimetallic Clusters

Sangmin Kim,[†] Florian Loose,[†] Máté J. Bezdek,[†] Xiaoping Wang[‡] and Paul J. Chirik*,[†]

[†]Department of Chemistry, Frick Laboratory, Princeton University, Princeton, NJ 08544, USA

[‡]Neutron Scattering Division, Neutron Sciences Directorate, Oak Ridge National Laboratory, Oak Ridge, TN 37831, USA

ABSTRACT: A rhodium-catalyzed method for the hydrogenation of *N*-heteroarenes is described. A diverse array of unsubstituted *N*-heteroarenes including pyridine, pyrrole and pyrazine, traditionally challenging substrates for hydrogenation, were successfully hydrogenated using the organometallic precatalysts, [(η^5-C_5Me_5)Rh(N-C)H] (N-C = 2-phenylpyridinyl (ppy) or benzo[h]quinolinyl (bq)). In addition, the hydrogenation of polyaromatic *N*-heteroarenes exhibited uncommon chemoselectivity. Studies into catalyst activation revealed that photochemical or thermal activation of [(η^5-C_5Me_5)Rh(bq)H] induced C(sp^2)–H reductive elimination and generated the bimetallic complex, [(η^5-C_5Me_5)Rh(μ$_2$,η^2-bq)Rh(η^5-C_5Me_5)H]. In the presence of H_2 both of the [(η^5-C_5Me_5)Rh(N-C)H] precursors and [(η^5-C_5Me_5)Rh(μ$_2$,η^2-bq)Rh(η^5-C_5Me_5)H] converted to a pentametallic rhodium hydride cluster, [(η^5-C_5Me_5)$_4$Rh$_5$H$_7$], the structure of which was established by NMR spectroscopy, X-ray and neutron diffraction. Kinetic studies on pyridine hydrogenation were conducted with each of the isolated rhodium complexes to identify catalytically relevant species. The data are most consistent with hydrogenation catalysis prompted by an unobserved multimetallic cluster with formation of [(η^5-C_5Me_5)$_4$Rh$_5$H$_7$] serving as a deactivation pathway.

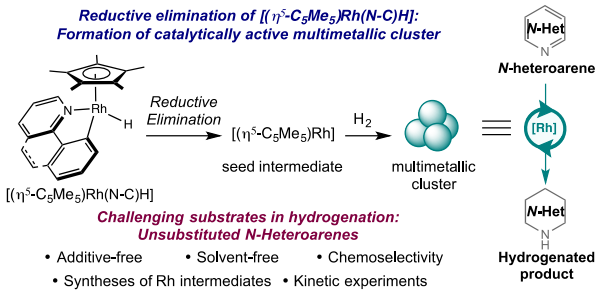

INTRODUCTION

N-Heterocycles are one of the most important and common substructures within pharmaceuticals with approximately 59% of the recent FDA-approved small molecule drugs containing such a ring.[1] As interest in drug discovery transitions from aromatic structure to those with more three dimensionality, so will interest for the synthesis of saturated *N*-heterocycles including piperidines, pyrrolidines and related structures (Scheme 1, a).[2] Current routes to these structures are less developed than their aromatic counterparts and as such the hydrogenation of *N*-heteroarenes has been of long standing interest.[3-5]

While advances have been made, including asymmetric variants,[3-5] this class of hydrogenation remains a challenge in contemporary catalysis due to poisoning by strongly coordinating nitrogen atoms or from the presence of weak C-H bonds adjacent to nitrogen atoms that promote deleterious side reactions.[6-8] As a result, most hydrogenations of this type are limited to polyaromatic *N*-heteroarenes such as quinoline and quinoxaline.[9-19] General methods for the hydrogenation of a broader subset of *N*-heteroarenes including pyridine, pyrrole, pyrimidine, pyridazine, or pyrazine have not been realized. In most successful cases, base additives or alcohols are required and conversions are low.[20] Discovery of additive-free catalysts with high turnovers and conversion would therefore be of value in synthesis.

Scheme 1. (a) Preparation of three-dimensional pharmacophores by hydrogenation of *N*-heteroarenes. (b) Arene hydrogenation with [(η^5-C_5Me_5)$RhCl_2$]$_2$ and catalytically active cluster. (c) Reductive elimination as a strategy to generate [(η^5-C_5Me_5)Rh] or [(η^5-C_5Me_5)RhH_2] for nucleation toward multimetallic cluster formation. (d) [(η^5-C_5Me_5)Rh(N-C)H] precatalysts.

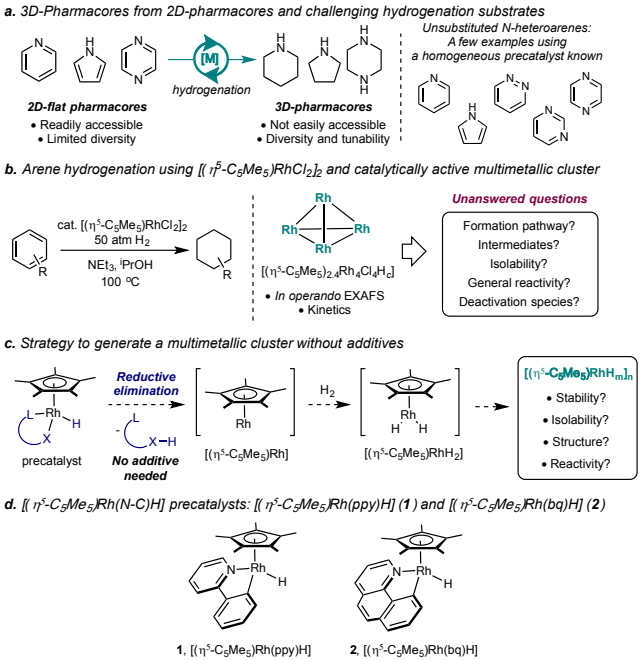

Table 1. (a) Scope of *N*-heteroarene hydrogenation promoted by 1.[a] (b) Catalytic deuteration of pyridine.

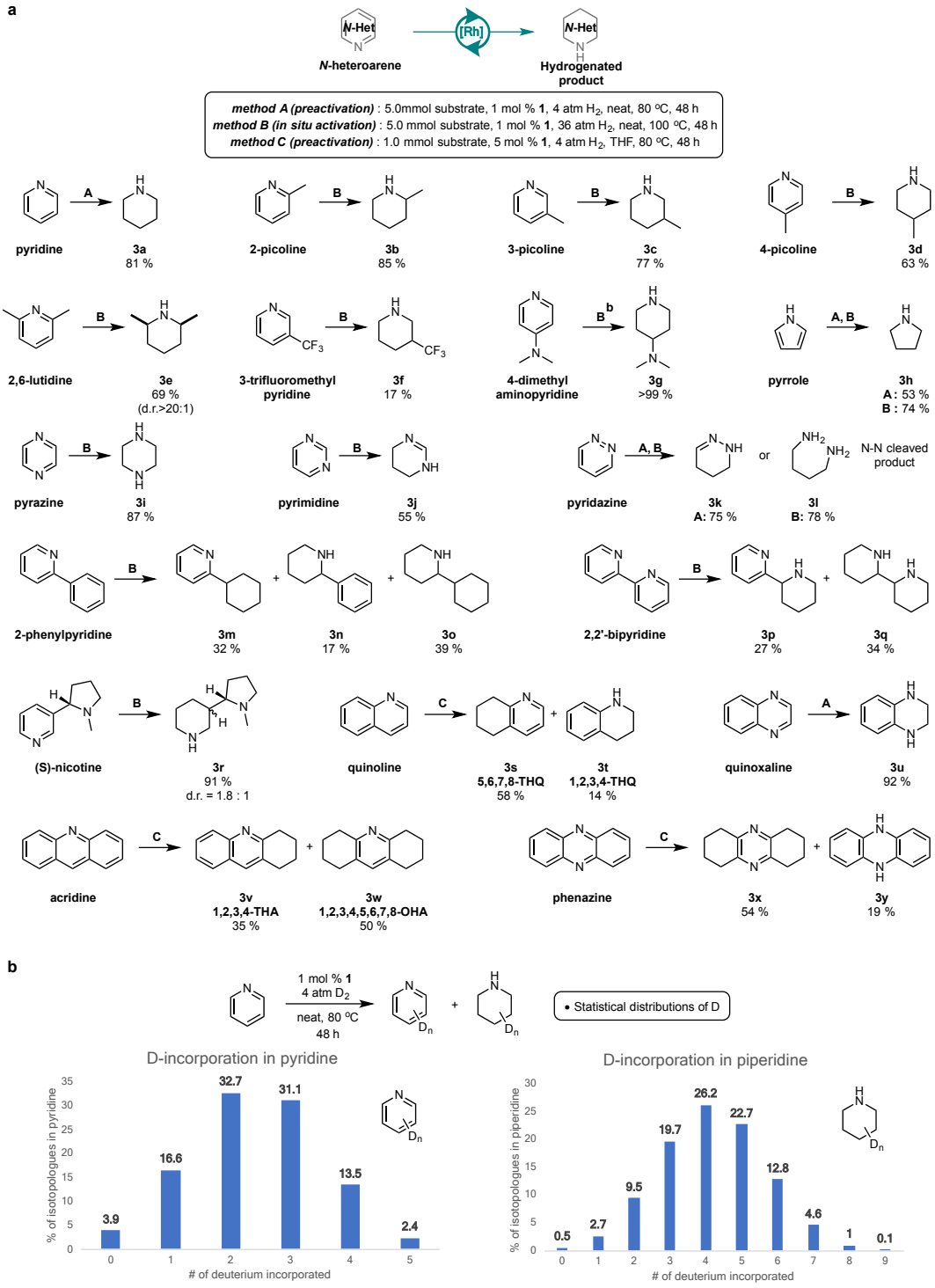

[a]Yields were determined by ^{1}H NMR spectroscopy using mesitylene as an internal standard. [b]5 mol% **1**, 1.0 mmol substrate (4-dimethylaminopyridine) and 1.0 mL THF.

Among various transition metals known to catalytically hydrogenate unsaturated organic compounds, rhodium is one of the most widely utilized in both homogeneous and heterogeneous catalysis.[21,22] It has recently been demonstrated that well-defined organometallic rhodium precatalysts such as $[(\eta^5\text{-}C_5Me_5)RhCl_2]_2$ or [(CAAC)Rh(COD)Cl] (CAAC = cyclic alkyl amino carbene, COD = 1,5-cyclooctadiene) promote the hydrogenation of selected arenes and heteroarenes.[23-26] Subsequent mechanistic studies on these catalytic mixtures have indicated that the organometallic rhodium compounds are converted into catalytically active multimetallic clusters or nanoparticles (Scheme 1, b).[27-31] While these multimetallic clusters have been definitively established as catalytically competent, rational generation and

modification of such species for improved performance remains a challenge.

As part of our broader program exploring the chemistry of [(η^5-C_5Me_5)Rh(ppy)H][32,33] as a catalyst for formation of N-H bonds by proton-coupled electron transfer (PCET),[34-36] the use of this complex as a precatalyst for *N*-heteroarene hydrogenation was of interest. Inspiration from studies on identification of [(η^5-C_5Me_5)$_{2.4}$$Rh_4Cl_4H_c$] formed from [($\eta^5$-$C_5Me_5$)$RhCl_2$]$_2$ as an active catalyst for arene hydrogenation[27-29] suggested that C(sp^2)–H reductive elimination of 2-phenylpyridine may provide a unique source of [(η^5-C_5Me_5)Rh]$_n$ or [(η^5-C_5Me_5)RhH_2]$_n$ compounds without the need for additives (Scheme 1, c).

Here we describe studies on the reductive elimination chemistry of [(η^5-C_5Me_5)Rh(ppy)H] (**1**, ppy = 2-phenylpyridinyl) and [(η^5-C_5Me_5)Rh(bq)H] (**2**, bq = benzoquinolinyl) (Scheme 1, d) and identification of multimetallic rhodium hydrides en route to nanoparticle formation. The resulting clusters proved active for the reduction of a range of *N*-heteroarenes many of which had not been previously hydrogenated and therefore open a new avenue in synthesis.

RESULTS AND DISCUSSION

Our studies commenced with evaluation of [(η^5-C_5Me_5)Rh(N-C)H] precatalysts for the additive-free hydrogenation of pyridine. Initial conditions employed 0.05 mmol of pyridine in THF-d_8 solution with 4 atm of H_2 at 60 °C with 0.16 mol% of **1** as the precatalyst. Monitoring the reaction by ^{1}H NMR spectroscopy revealed 11% conversion to piperidine (**3a**) in 24 hours. Performing the reaction on a preparative scale using neat pyridine with 4 atm of H_2 at 80 °C produced piperidine in 81% yield (Table 1, a). Because neat conditions produced optimal reactivity, other liquid substrates were evaluated under these conditions. In each case, 1-5 mol% of **1** was used along with 4 or 36 atm of H_2. Substituted pyridine derivatives including challenging substrates such as 3-picoline were successfully hydrogenated (**3b-g**). The electron-poor pyridine, 3-trifluoromethylpyridine, produced the desired piperidine (**3f**) in only 17% yield but it should be noted that fluorinated piperidines are not easily accessed by other methods.

Unsubstituted *N*-heteroarenes other than pyridine were also successful hydrogenated including examples that have not been hydrogenated previously (**3h-j**). With pyridazine, two different products were obtained depending on the conditions of the reaction (**3k, 3l**). The rhodium-catalyzed hydrogenation of substituted pyridines was also investigated including the bioactive molecule, (*S*)-nicotine (**3m-r**). Although high conversions were generally obtained, relatively poor chemoselectivity was observed between phenyl and pyridine rings of 2-phenylpyridine (**3m, 3n**).

Unusual chemoselectivity was observed in the hydrogenation of polyaromatic *N*-heteroarenes (**3s-y**). Most known partial reduction reactions of quinoline and acridine yield 1,2,3,4-tetrahydroquinoline and 1,10-dihydroacridine, respectively. However, with **1** as the precatalyst, 5,6,7,8-tetrahydroquinoline (**3s**) and 1,2,3,4,5,6,7,8-octahydroacridine (**3w**) were obtained as the major products in 58 and 50% yields, respectively, when THF was used as the solvent. Only one other example of this selectivity has been reported using a ruthenium hydride catalyst.[37,38] Hydrogenation of phenazine produced 1,2,3,4,6,7,8,9-octahydrophenazine (**3x**) as the major product in 54% yield analogous to the selectivity observed in acridine hydrogenation. Pyrazole and imidazole were unreactive given the endergonic nature of the hydrogenation at reaction temperature.[39,40] No reaction was also observed with 1,3,5-triazine and isoquinoline.

The catalytic deuteration of pyridine was examined using [(η^5-C_5Me_5)Rh(ppy)H] as a precatalyst (Table 1, b). With 1 mol% of **1** at 80 °C for 48 hours, formation of both deuterated piperidine and pyridine was observed with a statistical distribution of deuterium in both organic molecules. Analysis of the deuterated piperidine product by quantitative ^{13}C NMR spectroscopy revealed complex patterns, consistent with irregular stereochemistry and formation of various isotopomers and isotopologues (Figure S14). These results demonstrate that the *N*-heteroarene hydrogenation reaction involves rapid H–D exchange prior to deuteration and the insertion of the pyridine into the metal-hydride(deuteride) bonds is reversible.

The synthesis and catalytic PCET reactivity of **1** and **2** with organic substrates have been thoroughly investigated,[32,33] while our group has explored the role of **1** as a PCET catalyst to promote N-H bond-formation using H_2 as the stoichiometric hydrogen source.[34-36] Despite these studies and applications, little is known about the thermal stability of these compounds and their propensity to undergo reductive elimination. Recently, it was reported that [(η^5-C_5Me_5)Rh(bq)R] (R = 4-CF_3Ph, Me) undergoes reductive elimination by chemical oxidation but not under thermal conditions[41] but the reactivity of the corresponding hydride, **2** was not addressed in that study. Given the utility of **1** as a precatalyst with unique reactivity for *N*-heteroarene hydrogenation and the likely formation of clusters as the active species, the reductive elimination chemistry and thermal stability of both **1** and **2** was systematically investigated.

Monitoring the hydrogenation of pyridine with **1** in THF-d_8 by ^{1}H NMR spectroscopy resulted in the

observation of new rhodium hydride signals over 24 h (Figure S7, Supporting Information). Interestingly, these signals were also generated in THF-d_8 in the absence of pyridine, demonstrating that **1** is converted into *different* rhodium hydride derivatives under H_2. Notably, these new compounds form in the absence of base or alcohols, reagents typically required for multimetallic cluster formation.

Independent syntheses were conducted to identify the new rhodium hydride(s) formed under catalytic conditions. Irradiation of a THF-d_8 solution of **1** or **2** with blue light at ambient temperature or heating to 70 °C in the absence of H_2 resulted in formation of a new bimetallic complex as judged by ^{1}H NMR spectroscopy. Isolation of the bimetallic product obtained from **1** proved challenging due to rapid isomerization (*vide infra*) but the bimetallic product, [(η^5-C_5Me_5)Rh(μ_2,η^2-bq)Rh(η^5-C_5Me_5)H] (**4**) obtained from **2** was isolated and fully characterized by X-ray diffraction and NMR spectroscopy (Scheme 2). The hydride was located in the solid-state structure. Diamagnetic **4** contains two [(η^5-C_5Me_5)Rh] fragments with a Rh-Rh distance of 2.7306(2) Å and is best described as an adduct of [(η^5-C_5Me_5)RhH] with [(η^5-C_5Me_5)Rh(bq)]. The net loss of one benzoquinoline ligand, observed by NMR spectroscopy, supports C(sp^2)–H reductive elimination followed by dissociation of the *N*-heteroarene from the coordination sphere of one rhodium. Analysis of the NMR data following irradiation or thermolysis of **1** support formation of a similar bimetallic complex along with free phenylpyridine although the number of isomers and byproducts detected complicated definitive assignment.

Scheme 2. (a) Synthesis of the bimetallic complex, 4. (b) Solid state structure of 4 at 30% probability ellipsoids. Hydrogen atoms, except the Rh-H omitted for clarity.

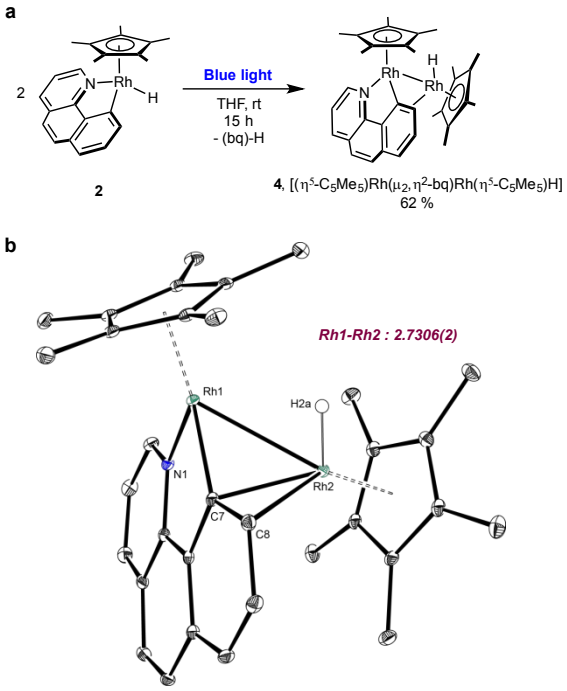

The observed loss of one of the supporting ligands upon photochemical or thermal activation of **1** or **2** prompted an additional deuterium labeling study. The rhodium deuteride **1-d_1** was prepared by the reaction of [(η^5-C_5Me_5)Rh(ppy)] and D_2 in THF for 30 min at 23 °C. Monitoring a THF-d_8 solution of the compound by ^{1}H NMR spectroscopy established rapid H-D exchange between the rhodium-hydride (deuteride) site and the aryl ligand, consistent with rapid C(sp^2)–H(D) reductive elimination, C–C bond rotation and oxidative addition (Scheme 3). The thermal or photochemical activation is therefore crucial for dissociation of ligand rather than for promoting the C–H bond forming step.

Scheme 3. Observation of H/D exchange on the ligand at room temperature under dark conditions.

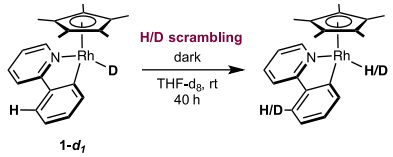

The photochemical and thermal stabilities of both **1** and **2** were studied to explore the possibility of ligand loss as a route to higher order rhodium hydride clusters. Irradiation with blue light or heating a THF-d_8 solution of either rhodium hydride to 70 °C under 4 atm of H_2 resulted in a color change from yellow to dark brown over the course of 30 minutes. Complete conversion was observed after 24 hours and analysis of the product mixture by ^{1}H NMR spectroscopy established liberation of free 2-phenylpyridine or benzo[h]quinoline along with formation of new η^5-C_5Me_5 and rhodium-hydride resonances (δ_{Rh-H} = -13.23, -14.14 and -22.73 ppm in

THF-d_8). Recrystallization from pentane at -35 ºC yielded brown crystals suitable for X-ray diffraction and neutron scattering. The combined NMR spectroscopic and crystallographic data support formation of a neutral pentametallic rhodium–hydride cluster, [(η^5-C_5Me_5)$_4$Rh$_5$H$_7$] (**5**) (Scheme 4). Unlike other transition metal clusters containing η^5-C_5Me_5 and hydride ligands, the complex has a unique structure comprised of a tetrahedral Rh_4 core with the additional rhodium at the apex.[42-50] Three of the rhodium atoms in the core are ligated by η^5-C_5Me_5 rings while the other is ligand free and capped by the unique [(η^5-C_5Me_5)Rh]. The bond distance of Rh4-Rh5 is significantly shorter than the other Rh–Rh bonds. All seven hydrides were successfully located by neutron diffraction (Scheme 4, b). Addition of 4 atm of D_2 gas to a benzene-d_6 solution containing [(η^5-C_5Me_5)$_4$Rh$_5$H$_7$] at ambient temperature resulted in rapid exchange in *all* of the metal hydride positions.

To assay whether the bimetallic complex, **4** was a precursor to the pentametallic cluster, **5**, a THF-d_8 solution of the former was exposed to 4 atm of H_2 and the progress of the reaction monitored by ^{1}H NMR spectroscopy. Over the course of 18 hours at ambient temperature, **5** was observed along with **2**, free benzo[h]quinoline and C_5Me_5H (Scheme 5, Figure S9). The observation of **2** supports hydrogenolysis of **4** to generate [(η^5-C_5Me_5)RhH$_2$] and [(η^5-C_5Me_5)Rh(N-C)H]. The formation of **5** implies one of the intermediates after hydrogenolysis, [(η^5-C_5Me_5)RhH$_2$], is related to its formation.

Scheme 4. (a) Synthesis of the pentametallic cluster, 5. (b) Solid state structure of 5 and expanded view of the Rh core at 30% probability ellipsoids. Hydrogen atoms, except the Rh-H omitted for clarity.

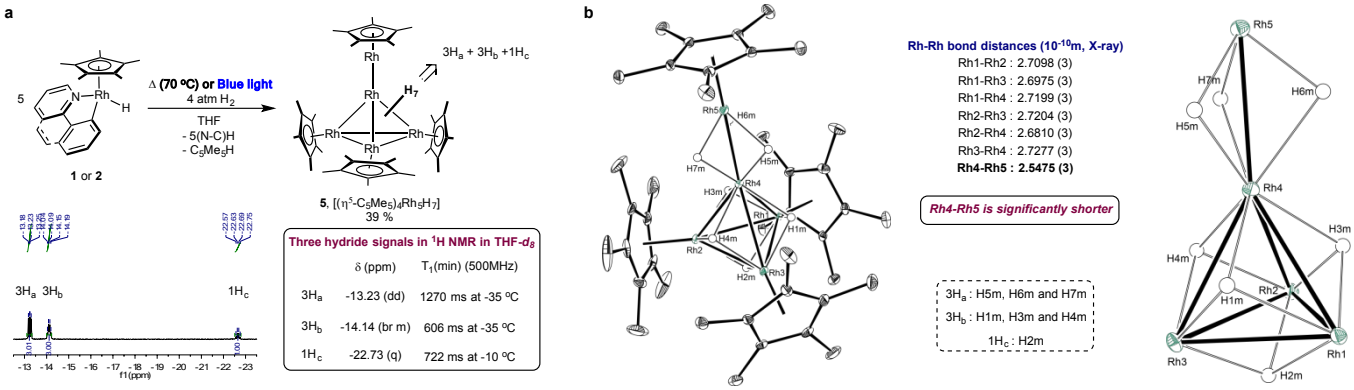

Scheme 5. Hydrogenolysis of 4 yielding 5 and the starting monometallic precatalyst, 2.

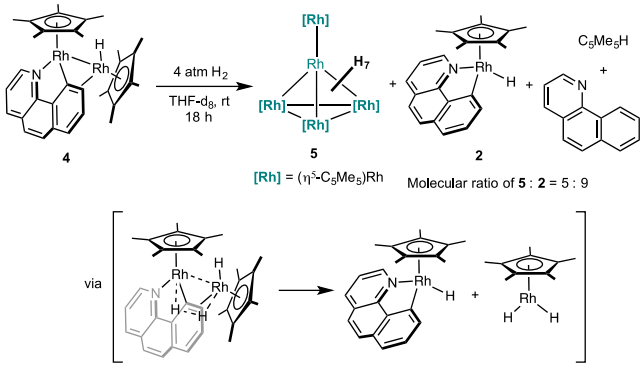

Based on the experimental observations, the most plausible pathway for formation of the cluster likely involves: (*i*) rapid, initial C(sp^2)–H reductive elimination to form [(η^5-C_5Me_5)Rh(I)(κ^1-N-C)]; (*ii*) dissociation of the neutral ligand by thermal or photochemical activation to yield transient [(η^5-C_5Me_5)Rh]; (*iii*) interaction of [(η^5-C_5Me_5)Rh] and [(η^5-C_5Me_5)Rh(N–C)H] to generate the bimetallic intermediate, [(η^5-C_5Me_5)Rh(μ_2,η^2-bq)Rh(η^5-C_5Me_5)H]; (*iv*) generation of [(η^5-C_5Me_5)RhH$_2$] and (*v*) the final formation of the cluster **5** by the aggregation of [(η^5-C_5Me_5)RhH$_2$] likely *via* [(η^5-C_5Me_5)$_3$Rh$_4$H$_7$] (Scheme 6). This pathway likely involves formation of [(η^5-C_5Me_5)Rh(I)] and [(η^5-C_5Me_5)RhH$_2$] by reductive elimination from [(η^5-C_5Me_5)Rh(N–C)H].

To identify the nature of the active species and gain insight into the mechanism of additive-free *N*-heteroarene hydrogenation, kinetic experiments using each of the isolated rhodium complexes were conducted (Figure 1). Pyridine was selected as a representative substrate and the rate of each reaction was determined by monitoring hydrogen uptake with 0.25 mol% of total rhodium (3.1 μmol of Rh) and 530 psi of H_2 at 78 ºC. The plots of H_2 uptake versus time are reported in the Supporting Information.

Examination of the kinetic profile when **1** was used as the precatalyst revealed a significant induction period within the first three hours and completion of the reaction after 28 h (Figure 1, a). Following the induction period, an exponential decay of the pyridine concentration was observed, signaling a first order dependence on the substrate, which was confirmed by the relationship between conversion vs. reaction rate (Figure 1, b). The induction period followed by the first-order kinetic behavior implies that the precatalyst is converted to a new rhodium species, which can be either a single metal center catalyst or a multimetallic cluster. The maximum reaction rate during the reaction was 23.3

psi$_{H2}$ h^{-1}. Performing the hydrogenation of pyridine in the presence of Hg(0) produced no conversion, consistent with a multimetallic cluster rather than a monometallic compound.[27-31]

A filtration test was also conducted whereby the crude reaction mixture following catalytic hydrogenation was passed through Celite to remove observed black particulates and the volatiles removed *in vacuo* and the rhodium residue was analyzed by ^{1}H NMR spectroscopy. Both the bimetallic complex and **5** were observed (Figure S10). With the recovered soluble rhodium residue, a second cycle of pyridine hydrogenation was conducted and the uptake of H_2 monitored (Figure 1, c). A rapid initial rate of 4.5 psi$_{H2}$ h^{-1} was observed until 3 h and the reaction rate was gradually increased up to 11.2 psi$_{H2}$ h^{-1} over the course of time (Figure S19). A fast initial rate was observed, suggesting that a homogeneous catalyst is operative at early reaction times. This behavior was also observed in rhodium-catalyzed arene hydrogenation where a multimetallic cluster was proposed as the most active species formed from the precatalyst.[28] The increasing reaction rate observed during pyridine hydrogenation is therefore likely a result of **1** and the bimetallic product being converted to the active species during the course of hydrogenation and subsequent interaction with substrate.

Using isolated bimetallic complex, **4** as the precatalyst, a similar kinetic profile to **1** was obtained (Figure 1, d). An induction period was observed in the first 3 hours followed by exponential decay. Fitting the exponential region produced the maximum reaction rate of 19.6 psi$_{H2}$ h^{-1}, similar to the value obtained with **1**. Completion of the hydrogenation was observed at 24 hours, slightly faster than with **1**. Again, first-order kinetics was observed after the induction period based on the relationship between conversion vs. reaction rate (Figure 1, e). In the proposed evolution of the rhodium complexes shown in Scheme 6, the intermediate [(η^5-C_5Me_5)RhH$_2$] can result either from [(η^5-C_5Me_5)Rh] that forms directly from reductive elimination of [(η^5-C_5Me_5)Rh(N–C)H] or from hydrogenolysis of **4**. Because of the similar kinetic behavior of **1** and **4**, it is likely that [(η^5-C_5Me_5)RhH$_2$] is related to formation of the active species.

Scheme 6. Proposed pathway of the cluster formation from the precatalyst based on the experimental observations.

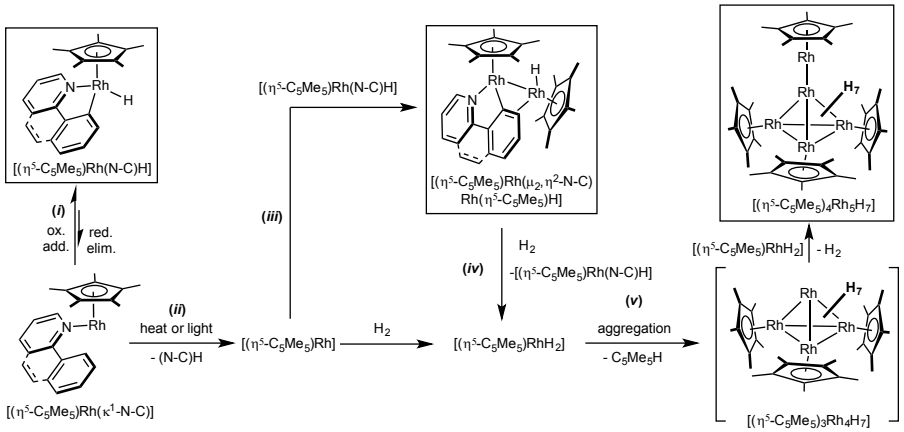

The kinetics of pyridine hydrogenation were evaluated using 0.05 mol% (0.25 mol% total rhodium) pentanuclear rhodium hydride cluster, [(η^5-C_5Me_5)$_4$Rh$_5$H$_7$] (Figure 1, f). Sigmoidal behavior was observed with relatively flat curvature and a completion time of 49 hours, significantly longer than the value obtained with **1**. Best fit of the plot yielded the maximum reaction rate of 8.5 psi$_{H2}$ h^{-1} which is distinctly lower than other kinetic data (Figure S23). A sigmoidal curve with an induction period indicates that **5** is converted into another catalytically active species. However, due to the significant difference in reactivity, the catalytic species from **5** can be eliminated at the most active catalyst during pyridine hydrogenation. The THF-d_8 ^{1}H NMR spectrum of the soluble Rh residue after the reaction revealed remaining **5** (Figure S11).

The insoluble rhodium black particulates were then recovered following pyridine hydrogenation initiated by **5** and was assayed for additional activity (Figure 1, g). The activity of this material was diminished from the initial sample **5** with a constant reaction rate of 4.8-5.3 psi$_{H2}$ h^{-1} for 30 h from the initial stage, best fit to the linear decrease of zero-order kinetics, a feature characteristic of heterogeneous catalysis, which implies catalytically active Rh(0) nanoparticles were generated from **5** (Figure S48). Although the reaction seems to be slower compared to the maximum reaction rate of **5**, it could be a result of decreased metal surface of nanoparticles by further agglomeration during recovery. Therefore, it is believed that **5** is further converted into a nanocluster which is catalytically active, but less reactive than the unidentified most active species generated from **1** and **4**.

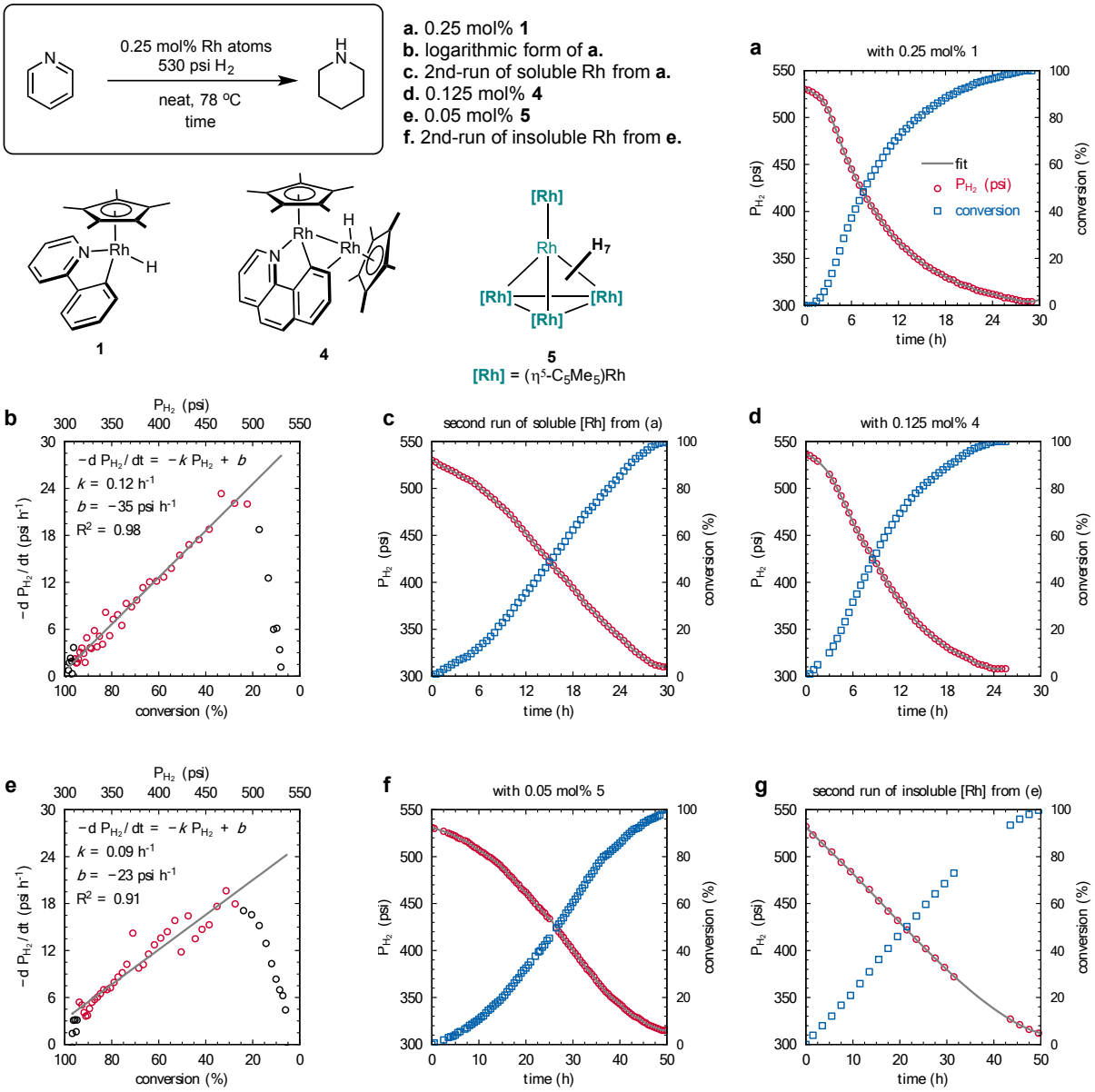

Figure 1. (a) Exponential decay of pyridine with a short induction period in pyridine hydrogenation using the precatalyst **1**. (b) First order kinetics of (a) after the induction period. (c) Kinetic profile using soluble Rh from (a). (d) Kinetic profile of pyridine hydrogenation using the bimetallic complex **4**. (e) First order kinetics of (d) after the induction period. (f) Kinetic profile of the reaction using the pentanuclear cluster **5**. (g) Kinetic profile of the second-run of (e).

Scheme 7. Evolution of the catalytically active species, catalyst deactivation and formation of nanoparticles based on synthetic and kinetic experiments.

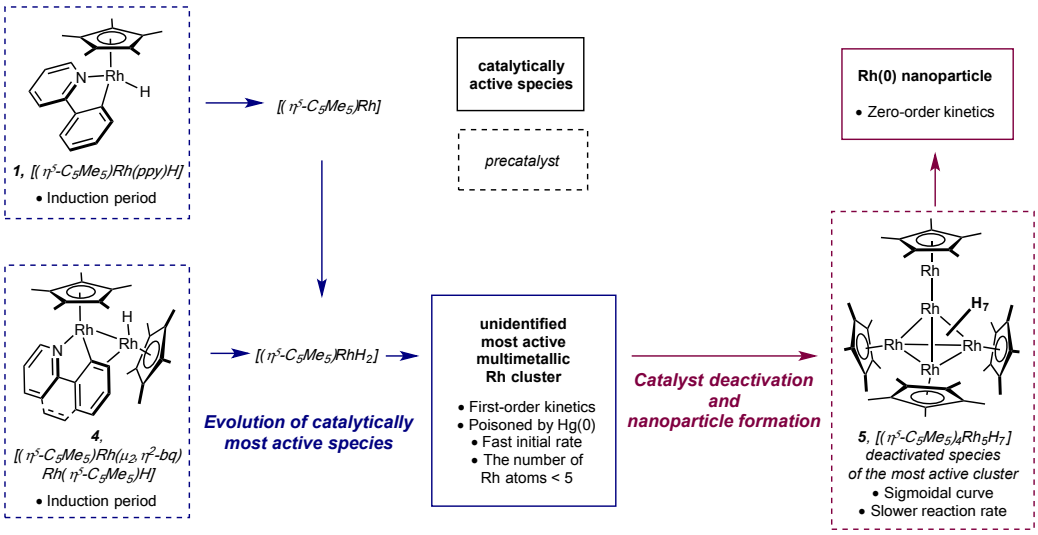

Analysis of all of the kinetic data and the various activities of the isolable rhodium complexes toward pyridine hydrogenation is summarized in Scheme 7. Because of the induction periods detected with [(η^5-C_5Me_5)Rh(ppy)H] (**1**) and [(η^5-C_5Me_5)Rh(μ_2,η^2-bq)Rh(η^5-C_5Me_5)H] (**4**), these compounds are the preferred precatalysts for the formation of most active catalytic species; likely a homogeneous multimetallic cluster. Support for this assignment derives from: *i*) the observed first-order behavior with respect to substrate, consistent with a single metal compound or a multimetallic cluster and not heterogeneous nanoparticle and *ii*) this catalyst (or a precursor to it) was poisoned by Hg(0), excluding a single metal compound. Because the cluster **5** was generated from **1** and **4** and inactive for pyridine hydrogenation, the most active species is likely formed prior to [(η^5-C_5Me_5)$_4$Rh$_5$H$_7$] and thus has less than five rhodium atoms. The most active catalytic species likely retains η^5-C_5Me_5 ligands given the molecular geometry of **5**. Such an organometallic cluster also may rationalize the observed chemoselectivity in the hydrogenation of polyaromatic substrates. The η^5-C_5Me_5 ligands likely create unique catalytically active sites that protect the core of the cluster and promote hydrogenation at the periphery. As such, the "outer" portions of polyaromatic substrates are preferentially reduced as in the case of 5,6,7,8-tetrahydroquinoline. This hypothesis needs to be validated with additional experimental and computational studies. Notably **5** can be further transformed into Rh(0) nanoparticles which are also catalytically active for pyridine hydrogenation as signaled by the zero-order dependence on substrate. Importantly the nanoparticles are *less* active than the rhodium aggregate formed prior to formation of **5**.

CONCLUSION

In summary, an additive-free hydrogenation of *N*-heteroarene using a homogeneous precatalyst [(η^5-C_5Me_5)Rh(N-C)H] has been discovered. Challenging substrates for hydrogenation, unsubstituted *N*-heteroarenes such as pyridine, pyrrole, pyrazine and 3-picoline, were reduced in high yields. Polyaromatics afforded unusual chemoselectivity, for example, yielding 5,6,7,8-tetrahydroquinoline or 1,2,3,4,5,6,7,8-octahydroacridine. To identify the catalytically active species, the bimetallic and pentametallic rhodium hydride complexes were separately synthesized from precatalysts and fully characterized. Following kinetic experiments using various rhodium complexes elucidated the evolution of catalytically active multimetallic cluster formed from [(η^5-C_5Me_5)Rh(N-C)H] or [(η^5-C_5Me_5)Rh(μ_2,η^2-bq)Rh(η^5-C_5Me_5)H]. This most active species was deactivated by forming the pentametallic cluster, but the pentametallic cluster was further converted to nanoparticles which are catalytically active, but less reactive than the most active multimetallic cluster.

This result shows that reductive elimination of precatalysts can lead to the formation of catalytically active multimetallic species without additives such as bases or alcohols. Our new strategic method for multimetallic cluster formation will be able to give a new chance for hydrogenation in medicinal and agrochemical and petroleum chemistry.

ASSOCIATED CONTENT

Supporting Information

The Supporting Information is available free of charge on the ACS Publications website at DOI: 10.1021/

AUTHOR INFORMATION

Corresponding Author

*pchirik@princeton.edu

ORCID

Paul J. Chirik: 0000-0001-8473-2898
Sangmin Kim: 0000-0002-7289-0693
Florian W. Loose: 0000-0003-1643-4607
Máté J. Bezdek: 0000-0001-7860-2894
Xiaoping Wang: 0000-0001-7143-8112

Notes

The authors declare no competing financial interest

ACKNOWLEDGMENT

This research was supported by the U.S. Department of Energy, Office of Science, Office of Basic Energy Sciences, Catalysis Science program, under Award DE-SC0006498. Single crystal neutron diffraction performed on TOPAZ used resources at the Spallation Neutron Source, a DOE Office of Science User Facility operated by the Oak Ridge National Laboratory, under Contract No. DE-AC05-00OR22725 with UT-Battelle, LLC. S.K. thanks Samsung Scholarship for financial support. F.L. acknowledges financial support from a DFG research fellowship (LO 2377/1-1). M.J.B. thanks the Natural Sciences and Engineering Research Council of Canada for a predoctoral fellowship (PSG-D) and Princeton University for a Porter Ogden Jacobus Honorific Fellowship. S.K. and P.J.C. acknowledge István Pelczer and Kenith Conover at Princeton University for measurement of T_1(min). The authors acknowledge the use of Princeton's Imaging and Analysis Center (IAC), which is partially supported by the Princeton Center for Complex Materials (PCCM), a National Science Foundation (NSF) Materials Research Science and Engineering Center (MRSEC; DMR-1420541). S.K. thanks Taeho Son and C. Rose Kennedy for plotting kinetic data and Hongyu Zhong for the ORTEP.

REFERENCES

(1) Vitaku, E.; Smith, D. T.; Njardarson, J. T. Analysis of the Structural Diversity, Substitution Patterns, and Frequency of Nitrogen Heterocycles among U.S. FDA Approved Pharmaceuticals. *J. Med. Chem.* **2014**, *57*, 10257-10274.

(2) Lovering, F.; Bikker, J.; Humblet, C. Escape from Flatland: Increasing Saturation as an Approach to Improving Clinical Success. *J. Med. Chem.* **2009**, *52*, 6752-6756.

(3) Wang, D.-S.; Chen, Q.-A.; Lu, S.-M.; Zhou, Y.-G. Asymmetric Hydrogenation of Heteroarenes and Arenes. *Chem. Rev.* **2012**, *112*, 2557-2590.

(4) Balakrishna, B.; Núñez-Rico, J. L.; Vidal-Ferran, A. Substrate Activation in the Catalytic Asymmetric Hydrogenation of N-Heteroarenes. *Eur. J. Org. Chem.* **2015**, 5293-5303.

(5) Chen, Z.-P.; Zhou, Y.-G. Asymmetric Hydrogenation of Heteroarenes with Multiple Heteroatoms. *Synthesis* **2016**, *48*, 1769-1781.

(6) Glorius, F. Asymmetric hydrogenation of aromatic compounds. *Org. Biomol. Chem.* **2005**, *3*, 4171-4175.

(7) Perrin, L.; Werkema, E. L.; Eisenstein, O.; Anderson, R. A. Two $[1,2,4\text{-}(Me_3C)_3C_5H_2]_2CeH$ Molecules are Involved in Hydrogenation of Pyridine to Piperidine as Shown by Experiments and Computations. *Inorg. Chem.* **2014**, *53*, 6361-6373.

(8) Crabtree, R. H. Deactivation in Homogeneous Transition Metal Catalysis: Causes, Avoidance, and Cure. *Chem. Rev.* **2015**, *115*, 127-150.

(9) Dobereiner, G. E.; Nova, A.; Schley, N. D.; Hazari, N.; Miller, S. J.; Eisenstein, O.; Crabtree, R. H. Iridium-Catalyzed Hydrogenation of N-Heterocyclic Compounds under Mild Conditions by an Outer-Sphere Pathway. *J. Am. Chem. Soc.* **2011**, *133*, 7547-7562.

(10) Sridharan, V.; Suryavanshi, P. A.; Menendez, J. C. Advances in the Chemistry of Tetrahydroquinolines. *Chem. Rev.* **2011**, *111*, 7157-7259.

(11) Liu, Y.; Du, H. Metal-Free Borane-Catalyzed Highly Stereoselective Hydrogenation of Pyridines. *J. Am. Chem. Soc.* **2013**, *135*, 12968-12971.

(12) Wu, J.; Barnard. J. H.; Zhang, Y.; Talwar, D.; Robertson, C. M.; Xiao, J. Robust cyclometallated Ir(III) catalysts for the homogeneous hydrogenation of N-heterocycles under mild conditions. *Chem. Comm.* **2013**, *49*, 7052-7054.

(13) Mahdi, T.; Nathaniel del Castillo, J.; Stephan, D. W. Metal-Free Hydrogenation of N-Based Heterocycles. *Organometallics*, **2013**, *32*, 1971-1978.

(14) Chakraborty, S.; Brennessel, W. W.; Jones, W. D. A Molecular Iron Catalyst for the Acceptorless Dehydrogenation and Hydrogenation of N-Heterocycles. *J. Am. Chem. Soc.* **2014**, *136*, 8564-8567.

(15) Zhang, Z.; Du, H. A Highly *cis*-Selective and Enantioselective Metal-Free Hydrogenation of 2,3-Disubstituted Quinoxalines. *Angew. Chem,. Int. Ed.* **2015**, *54*, 623-626.

(16) Xu, R.; Chakraborty, S.; Yuan, H.; Jones, W. D. Acceptorless, Reversible Dehydrogenation and Hydrogenation of N-Heterocycles with a Cobalt Pincer Catalyst. *ACS Catal.* **2015**, *5*, 6350-6354.

(17) Zhang, Z.; Du, H. Enantioselective Metal-Free Hydrogenations of Disubstituted Quinolines. *Org. Lett.* **2015**, *17*, 6266-6269.

(18) Ji, Y.-G.; Wei, K.; Liu, T.; Wu, L.; Zhang, W.-H. "Naked" Iridium(IV) Oxide Nanoparticles as Expedient and Robust Catalysts for Hydrogenation of Nitrogen Heterocycles: Remarkable Vicinal Substitution Effect and Recyclability. *Adv. Synth. Catal.* **2017**, *359*, 933-940.

(19) Adam, R.; Cabrero-Antonino, J. R.; Spannenberg, A.; Junge, K.; Jackstell, R.; Beller, M. A General and Highly Selective Cobalt-Catalyzed Hydrogenation of N-Heteroarenes under Mild Reaction Conditions. *Angew. Chem., Int. Ed.* **2017**, *56*, 3216-3220.

(20) Jardine, I.; McQuillin, F. J. Homogeneous Hydrogenation of the -N=N-, -CH=N-, and $-NO_2$ Groupings. *Chem. Commun.* **1970**, 626.

(21) Zweifel, G. S.; Nantz, M. H. Ch5. Functional Group Transformations: The Chemistry of Carbon-Carbon π-Bonds and Related Reactions, Modern Organic Synthesis, Wiley, 2006.

(22) Frediani, P.; Pistolesi, V.; Frediani, M.; Rosi, L. Catalytic activity of dihydride ruthenium complexes in the hydrogenation of nitrogen containing heterocycles. *Inorg. Chim. Acta* **2006**, *359*, 917-925.

(23) Russell, M. J.; White, C.; Maitlis, P. M. Stereoselective Homogeneous Hydrogenation of Arenes to Cyclohexanes Catalysed by $[Rh(\eta^5\text{-}C_5Me_5)Cl_2]_2$. *J. Chem. Soc., Chem. Commun.* **1977**, 427-428.

(24) Gill, D. S.; White, C.; Maitlis, P. M. Pentamethylcyclopentadienyl-rhodium and -iridium complexes. Part 16. Homogeneous hydrogenation catalysts. *J. Chem. Soc., Dalton Trans.* **1978**, 617-626.

(25) Nairoukh, Z.; Wollenburg, M.; Schlepphorst, C.; Bergander, K.; Glorius, F. The formation of all-cis-(multi)fluorinated piperidines by a dearomatization-hydrogenation process. *Nat. Chem.* **2019**, *11*, 264-270.

(26) Wiesenfeldt, M. P.; Nairoukh, Z.; Dalton, T.; Glorius, F. Hydrogenation of Borylated Arenes. *Angew. Chem., Int. Ed.* **2019**, *58*, 6549-6553.

(27) Hagen, C. M.; Widegren, J. A.; Maitlis, P. M.; Finke, R. G. Is It Homogeneous or Heterogeneous Catalysis? Compelling Evidence for Both Types of Catalysts Derived from $[Rh(\eta^5\text{-}C_5Me_5)Cl_2]_2$ as a Function of Temperature and Hydrogen Pressure. *J. Am. Chem. Soc.* **2005**, *127*, 4423-4432.

(28) Bayram, E.; Linehan, J. C.; Fulton, J. L.; Roberts, J. A. S.; Szymczak, N. K.; Smurthwaite, T. D.; Özkar, S.; Balasubramanian, M.; Finke, R. G. Is It Homogeneous or Heterogeneous Catalysis Derived from $[RhCp^*Cl_2]_2$? *In Operando* XAFS, Kinetic, and Crucial Kinetic Poisoning Evidence for Subnanometer Rh_4 Cluster-Based Benzene Hydrogenation Catalysis. *J. Am. Chem. Soc.* **2011**, *133*, 18889-18902.

(29) Bayram, E.; Linehan, J. C.; Fulton, J. L.; Szymczak, N. K.; Finke, R. G. $[RhCp^*Cl_2]_2$ Precatalyst System: Is it Single-Metal Rh_1Cp^*-Based, Subnanometer Rh_4 Cluster-Based, or $Rh(0)_n$ Nanoparticle-Based Cyclohexene Hydrogenation Catalysis at Room Temperature and Mild Pressures? *ACS Catal.* **2015**, *5*, 3876-3886.

(30) Tran, B. L.; Fulton, J. L.; Linehan, J. C.; Lercher, J. A.; Bullock, R. M. Rh(CAAC)-Catalyzed Arene Hydrogenation: Evidence for Nanocatalysis and Sterically Controlled Site-Selective Hydrogenation. *ACS Catal.* **2018**, *8*, 8441-8449.

(31) Tran, B. L.; Fulton, J. L.; Linehan, J. C.; Balasubramanian, M.; Lercher, J. A.; Bullock, R. M. Operando XAFS Studies on Rh(CAAC)-Catalyzed Arene Hydrogenation. *ACS Catal.* **2019**, *9*, 4106-4114.

(32) Hu, Y.; Shaw, A. P.; Norton, J. R.; Sattler, W.; Rong, Y. Synthesis, Electrochemistry, and Reactivity of New Iridium(III) and Rhodium(III) Hydrides. *Organometallics* **2012**, *31*, 5058-5064.

(33) Hu, Y.; Norton, J. R. Kinetics and Thermodynamics of H^-/H•/H^+ Transfer from a Rhodium(III) Hydride. *J. Am. Chem. Soc.* **2014**, *136*, 5938-5948.

(34) Pappas, I.; Chirik, P. J. Ammonia Synthesis by Hydrogenolysis of Titanium-Nitrogen Bonds Using Proton Coupled Electron Transfer. *J. Am. Chem. Soc.* **2015**, *137*, 3498-3501.

(35) Pappas, I.; Chirik, P. J. Catalytic Proton Coupled Electron Transfer from Metal Hydrides to Titanocene Amides, Hydrazides and Imides: Determination of Thermodynamic Parameters Relevant to Nitrogen Fixation. *J. Am. Chem. Soc.* **2016**, *138*, 13379-13389.

(36) Bezdek, M. J.; Chirik, P. J. Pyridine(diimine) Chelate Hydrogenation in a Molybdenum Nitrido Ethylene Complex. *Organometallics* **2019**, *38*, 1682-1687.

(37) Borowski, A. F.; Sabo-Etienne, S.; Donnadieu, B.; Chaudret, B. Reactivity of the Bis(dihydrogen) Complex $[RuH_2(\eta^2\text{-}H_2)_2(PCy_3)_2]$ toward N-Heteroaromatic Compounds. Regioselective Hydrogenation of Acridine to 1,2,3,4,5,6,7,8-Octahydroacridine. *Organometallics* **2003**, *22*, 1630-1637.

(38) Borowski, A. F.; Vendier, L.; Sabo-Etienne, S.; Rozycka-Sokolowska E.; Gaudyn, A. V. Catalyzed hydrogenation of condensed three-ring arenes and their N-heteroaromatic analogues by a bis(dihydrogen) ruthenium complex. *Dalton Trans.* **2012**, *41*, 14117-14125.

(39) Clot, E.; Eisenstein, O.; Crabtree, R. H. Computational structure-activity relationships in H_2 storage: how placement of N atoms affects release temperatures in organic liquid storage materials. *Chem. Commun.* **2007**, 2231-2233.

(40) Crabtree, R. H. Hydrogen storage in liquid organic heterocycles. *Energy Environ. Sci.* **2008**, *1*, 134-138.

(41) Kim, J.; Shin, K.; Jin, S.; Kim, D.; Chang, S. Oxidatively Induced Reductive Elimination: Exploring the Scope and Catalyst Systems with Ir, Rh, and Ru Complexes. *J. Am. Chem. Soc.* **2019**, *141*, 4137-4146.

(42) Churcill, M. R.; Ni, S. W.-Y. Crystal Structure and Location of the Bridging Hydride Ligand in μ-Chloro-μ -hydrido-bis[chloro(pentamethylcyclopentadienyl)rhodium(III)], a Homogeneous Hydrogenation Catalyst. *J. Am. Chem. Soc.* **1973**, *95*, 2150-2155.

(43) Espinet, P.; Bailey, P. M.; Piraino,P.; Maitlis, P. M. (Pentamethylcyclopentadienyl)rhodium and -iridium Complexes. 24.[1] Preparation, X-ray Crystal Structure, and Properties of $[Rh_4(\eta^5\text{-}C_5Me_5)_4H_4]^{2+}$. *Inorg. Chem.* **1979**, *18*, 2706-2710.

(44) Suzuki, H. Synthesis, Structure, and Chemistry of a Dinuclear Tetrahydride-Bridged Complex of Ruthenium, $(\eta^5\text{-}C_5Me_5)Ru(\mu\text{-}H)_4Ru(\eta^5\text{-}C_5Me_5)$. C-H Bond Activation and Coupling Reaction of Ethylene on Dinuclear Complexes. *Organometallics* **1994**, *13*, 1129-1146.

(45) Ohki, Y.; Uehara, N.; Suzuki, H. Pentanuclear Polyhydride Cluster of Ruthenium with Trigonal-Bipyramidal Geometry. Synthesis and Fluxional Behavior. *Organometallics* **2003**, *22*, 59-64.

(46) Nakajima, Y.; Kameo, H.; Suzuki, H. Cleavage of Nitrogen-Hydrogen Bonds of Ammonia Induced by Triruthenium Polyhydrido Clusters. *Angew. Chem., Int. Ed.* **2006**, *45*, 950-952.

(47) Shima, T.; Sugimura, Y.; Suzuki, H. Heterometallic Trinuclear Polyhydrido Complexes Containing Ruthenium and a Group 9 Metal, $[Cp^*_3Ru_2M(\mu_3\text{-}H)(\mu\text{-}H)_3]$ (M = Ir or Rh; $Cp^* = \eta^5\text{-}C_5Me_5$): Synthesis, Structure, and Site Selectivity in Reactions with Phosphines. *Organometallics* **2009**, *28*, 871-881.

(48) Shima, T.; Hu, S.; Luo, G.; Kang, X.; Luo, Y.; Hou, Z. Dinitrogen Cleavage and Hydrogenation by a Trinuclear Titanium Polyhydride Complex. *Science* **2013**, *340*, 1549-1552.

(49) Hu, S.; Shima, T.; Hou, Z. Carbon-carbon bond cleavage and rearrangement of benzene by a trinuclear titanium hydride. *Nature* **2014**, *512*, 413-415.

(50) Kameo, H.; Ito, Y.; Shimogawa, R.; Koizumi, A.; Chikamori, H.; Fujimoto, J.; Suzuki, H.; Takao, T. Synthesis and characterization of tetranuclear ruthenium polyhydrido clusters with pseudo-tetrahedral geometry. *Dalton Trans.* **2017**, *46*, 5631-5643.

Insert Table of Contents artwork here